

Research Article

Electrodeposited CdS Nanoparticles as Photocatalysts for Methyl Orange Removal

Hayder Khudhair Khattar^{1*}¹ College of Health and Medical Techniques, Al-Furat Al-Awsat Technical University, 54001 an-Najaf, Iraq.*Corresponding author: haider.khattarckm11@atu.edu.iq


Article Info

Keywords: Electrochemical Deposition, Photocatalytic Degradation, CdS NPs Thin Film.

Received: 01.11.2025

Accepted: 20.11.2025

Published: 25.11.2025

 © 2025 by the author's. The terms and conditions of the Creative Commons Attribution (CC BY) license apply to this open access article.

Abstract

Cadmium sulphide CdS NPs thin films were synthesized by electrochemical deposition using a two electrode, aluminum as the cathode (working electrode/substrates) and the inert graphite as anode (counter electrode). The electrolyte contained Cd (NO₃)₂·4H₂O (0.7 M), Thiourea (CH₄N₂S) (0.7 M), and Sodium sulfate Na₂SO₄ (0.1 M), and the PH was adjusted to 8 with (0.1 M) KOH, increasing deposition time and current density led thicker and higher-quality CdS thin film, obtained within the voltage range of 2-5 V. The photocatalytic performance of CdS thin film was evaluated utilize methyl orange (MO) as a model contaminant. A maximum decolorization efficiency of 90% was achieved for 5 ppm MO solution. The degradation followed pseudo-first-order kinetics according to the Langmuir–Hinshelwood model. UV-vis analysis in the existence of CdS NPs thin film. The Structural and surface characterization using XRD, UV-Vis, EDX and SEM, confirming the formation of well-defined CdS nanoparticales with good photocatalytic activity.

1. Introduction

Because of its various applications, thin film attracted the attention of many researchers, such as those working on semiconnected devices, photovoltaics, optoelectronic devices, electronic devices, radiation detectors, lasers, thermoelectric devices, and solar energy converters [1]. Photoelectrochemically (PEC) solar cells have been used, it may pay attention to the transformation of low energy to open broad research horizons in the field of semiconductor conductor materials of appropriate cost, and recent research has shown that the cadmium chalcogenide group (CdSe, CdS, CdTe) corresponds to this case [2]. The CdS material has a band gap energy of about 2.42 eV [3]. In low-cost solar cell applications, polycrystalline electrodes are of economic benefit. Thus, this study focused on the CDS thin film in polycrystalline nature. A number of researchers work in the field of investigating the photoelectrochemical property of CdS single crystal. A number of workers in this field succeeded in depositing CdS thin films through the electrochemical deposition technique, that is, by using two electrical poles. In this study, CDS films are prepared by the electrochemical deposition technique by two electrical systems on an aluminum substrate stainless resistant, which enables the thin film for descriptive studies such as structural, surface composition, surface morphology, and electrical properties. Photocatalytic Degradation [4]. For the semiconductor to be strong and effective in the degradation of different dyes, it must have an appropriate energy gap with perfect absorption properties in the visible light range. Cadmium sulfide (CdS) nanoparticles from group II–VI semiconductor nanocrystals are considered the most proper binary semiconductor because they are a material with a direct and broad band gap, are easy to prepare, and have a sufficient absorption coefficient, which makes them distinctive and of high value [5, 6]. Looking at the photocatalytic characteristics you possess, CdS nanoparticles are at most utilized for the decontamination of several dye-contaminated waters with other toxic materials [7–9]. Among a number of dyes, MO is very deleterious and widely applied in textiles, foodstuffs, paper,

and skin manufacture [10, 11]. Use effectively in such a study. It is considered the liberation of MO in the ambience to pollute river water. Therefore, it must be removed as an unwanted pollutant from water to be useful for use. The presence of these dyes in such places and water can cause their risk to human health, as well as animals [12, 13]. Consequently, decolorization of MO is most essential in the water decontamination process. Here, the factor that can affect photocatalytic activity is the CdS NPs thin film, through their size, structural shape, energy gap, and surface space [5, 7, 9, 14, 15]. The prepared CdS nanocrystals have been characterized by Field Emission Scanning Electron Microscopy (FESEM), X-ray Diffraction (XRD), UV-visible spectroscopy, and energy dispersive X-ray spectroscopy (EDX) during analysis of structural properties. Then, absorption spectra and emission spectra are examined for the decolorization of MO dye in the presence of CdS NPs thin film under a visible light lamp.

2. Experimental Method

The electrochemical method used to deposit a thin film of CdS NPs, by two electrode poles, In a 100 ml capacity cell, the aluminum pole is used as a cathode (working electrode), and the inert graphite pole is used as an anode (counter electrode) ($2\text{ cm} \times 2\text{ cm} \times 0.25\text{ mm}$) for each pole. The criteria used in this experience were included in Table 1. The pH used in this experience tends to the base a little using a KOH solution to reach the pH=8. In this process, we will be obtaining the sediment as well as thin films of CdS NPs deposited on the cathode aluminum plate electrode. During a 2-hour period of time at a temperature of 50°C and an electrical current preparation. The device used in the operation is 5000 milliamper (mA) maximum current and 30 volts (V) maximum voltage (China) and is used in this method as a magnetic engine in order to mix the materials by stirring. The distance was 2 cm between two plates. After the sedimentation process, the substrate was cleaned with deionized water. Through the observation viewing, a very regular and quite adherent reddish-yellowish film of CdS happens. In addition to a small deposit of CdS NPs, it is washed several times with deionized water, then with ethanol, to be dried at 60°C [16]. The calculated increase kinetics were studied via the variable precipitation parameters as the pH of the electrolytic bath and precipitation time (min). Analyzed chemical bonding by EDX, XRD, and UV techniques. The thin film of CdS was further characterized by FESEM.

Table 1: Material and measurement and parameters used in CdS NPs synthesis

Chemicals	Parameters
$\text{Cd}(\text{NO}_3)_2 \cdot 4\text{H}_2\text{O}$ (99% Thomas ,Indi)	0.7 M
KOH (99% Thomas ,Indi)	0.01 M
$\text{CH}_4\text{N}_2\text{S}$ (99% Thomas ,Indi)	0.7 M
Na_2SO_4 (99% Thomas ,Indi)	0.1 M
Deionized water	$0.7\ \mu\text{S}/\text{cm}$
pH	8
Temperature	$40\text{-}50\ ^\circ\text{C}$
Current density	$500\text{ mA}/\text{m}^2$
Al (2 cm^2) Cathode area	8 cm^2
Graphite (2 cm^2) Anode area	8 cm^2
Current density	4 A
Voltage/time	2-5 V/120 (min)

3. Result and Discussion

The application of the electric field through the working and counter pole a formation of CdS thin film, the inert electrode (graphite) as anode, which is considered the counter electrode, and the cathodic aluminum electrode (substrate), which is considered as the work electrode, use $\text{Cd}(\text{NO}_3)_2 \cdot 4\text{H}_2\text{O}$ as an electrolyte with a 0.7 M concentration, as well as thiourea ($\text{CH}_4\text{N}_2\text{S}$) with a 0.7 M concentration and sodium sulfate (Na_2SO_4) with a 0.1 M concentration. The electrolyte solution was a gradual addition from 0.1 M KOH to reach the base of pH=8. Before the precipitation process, the smooth surface of the substrate is cleaned with deionized water. The distance used in this process between the work electrode and the counter electrode was 2 cm^2 . During the sedimentation of materials, through the theoretical viewing of the electrolyte solution and the electrical precipitation process, we notice the process of adhesion that sediments on the smooth surface of the aluminum work electrode (substrate). With a sedimentation at the bottom of the electrical cell from the CDS yellow to reddish in a small amount, The thickness of the thin film is increasing with the time period used for sedimentation. The film thickness was about $200\ \mu\text{m}$ at 240 min as precipitation time. The current intensity, which changed from 2 to $5\text{ mA}/\text{cm}^2$ during the sedimentation process, was calcined at 200°C to get purity and eliminate impurities.

3.1. X-ray diffraction XRD

Through the XRD test, the grain size was specified by the Scherer equation $d=0.9\lambda/\beta\cos\theta$. The grain size was determined to be 10.7 nm, for nanoparticles and thin film. More technologies have been used to determine the shape and size by using the FESEM test; it indicates the CdS film formation uniformly on top of the aluminum plate with crystalline in nature [17]. can be visible in Figure 1. It display four strength peaks in the 2θ range, with values of 23.9° , 27.4° , 44.2° , and 66.9° . agree to JCPDS card number (96-900-8863), these peaks are the (100), (101), (110) and (203) crystallographic planes. They aid gain the spherical shape of CdS NPs. The presence of these wide peaks suggests that the granules exhibit either a high degree of amorphousness or fractional crystallinity. The dilation of the XRD peaks signal a small particle size and a non-uniform divide of particle sizes [18].

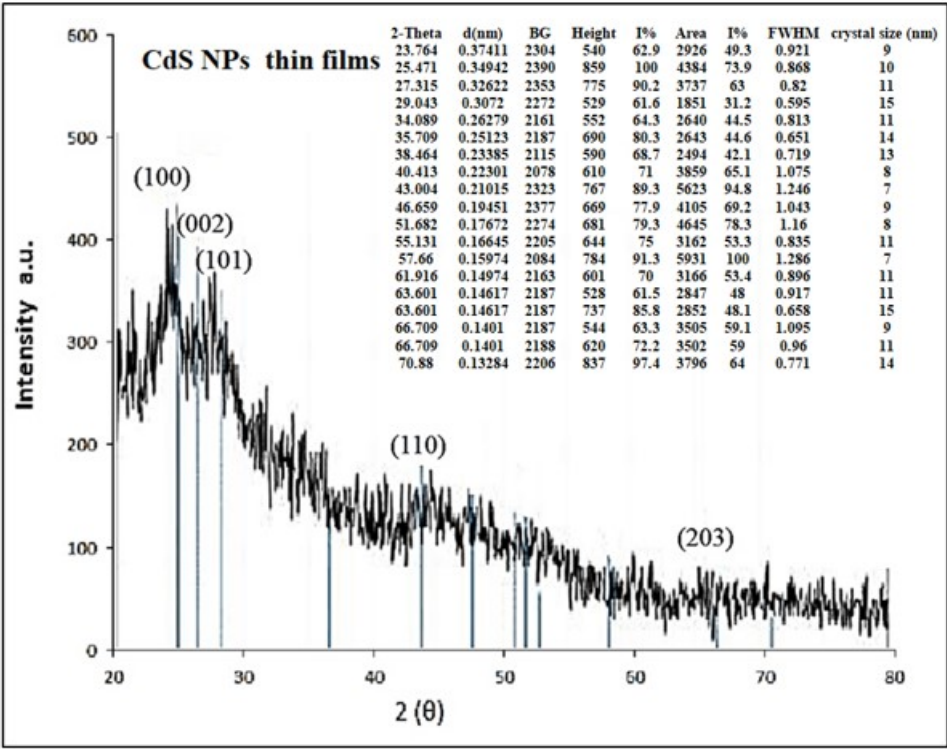


Figure 1: X-ray diffraction (XRD) for CdS thin film deposited on Aluminum substrates

3.2. Energy dispersive X-ray (EDX) spectroscopy

Figure 2 shows the typical EDX spectra of the designed CdS pattern. The EDX spectrum of the pure CdS specimen assures the chemical purity of the specimen, with strong peaks attached to Cd and S being obtained. The percentage of the atomic weight of sulfur was 44.7%, and the percentage of the atomic weight of Cd was 55.3%.

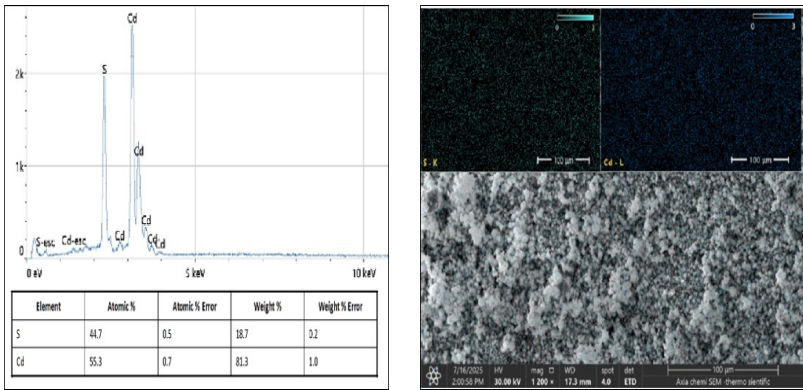


Figure 2: EDX analysis of CdS nanoparticles. for each Cd and S in the model for (CdS) NPs, For Cd=44.7 atomic%, S=55.3 atomic%

3.3. UV-visible Spectroscopy

Optical properties of the prepared sample using UV-visible spectroscopy have been discussed in the range of wavelengths from 200 to 600 nm at room temperature. CdS nanoparticles’ optical absorption spectra as well as band gap (2.4 eV) are accounted for as in Figure 3. The prepared nanoparticles’ optical bandgap was calculated through the Tauc equation, as given via equation ($\alpha h\nu=A(h\nu-E_g)^n$) [19].

3.4. Field Emission Scanning Electron Microscopy (FESEM)

The SM technology used the CdS samples prepared in the electrochemical method in Figure 4, where it was observed that the granules were spherical in shape and that the molecules crystallized well and distributed with CdS nanocrystals, which were much aggregated, due to the lack of capping agent in the composition process, and in this case it was observed that there was an excess in the size of the nanoparticles (27.69-49.17 nm) [20].

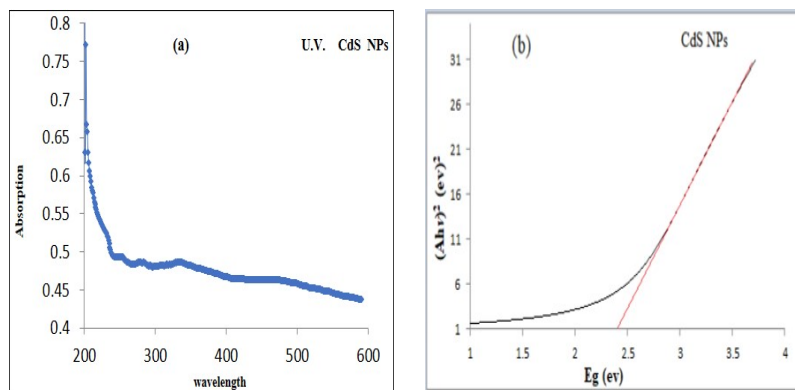


Figure 3: Absorption uv-visible spectroscopy spectrum (a) and bandgap (b) of CdS nanocrystals

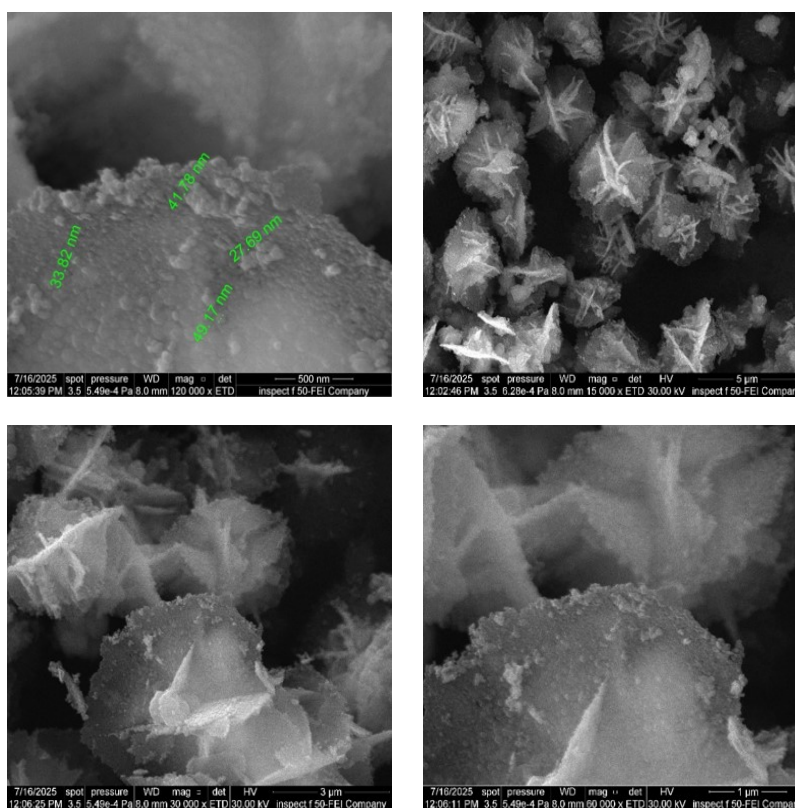


Figure 4: FESEM images: Cross-section of CdS NPs As prepared (5 μ m), (3 μ m), (1 μ m), (500 nm) The size of the nanoparticles reached (27.69-49.17) nm

4. Photocatalytic Method

4.1. Effective visual particles of CdS with MO dye

The UV/Vis absorption spectra of MO are indicated in Figure 5. MO displays (2) special absorption peaks at 271 nm and 464 nm, which agree with the “-N=N-” bonding for the azo group and the ring of benzene for MO, respectively, and MO possesses an orange color in the absorption peak specified at 464 nm (Thomas Baker, Mumbai, India), (UV-1900i Plus spectrophotometer) [21].

Figure 5 Plot of absorbance as a function of wavelength (nm) for methyl orange concentration was 15 ppm (λ_{max} =464 nm). Figure 5 shows the color degradation procedure for the methyl orange (MO) solution under the influence of the ultraviolet radiation system only. The test method contains 100 ml of a solution with a concentration of 15 parts per million. The empty experiment showed, under the ultraviolet radiation without the presence of a photocatalyst, that the rate of direct photodegradation was minimal during a 240-minute treatment period. UV rays the color removal can partially occur by physical absorption on the CdS nanoparticles after 240 minutes. So, the color degradation depends on all of the absorption processes and photocatalysis of the CdS nanoparticles [22, 23].

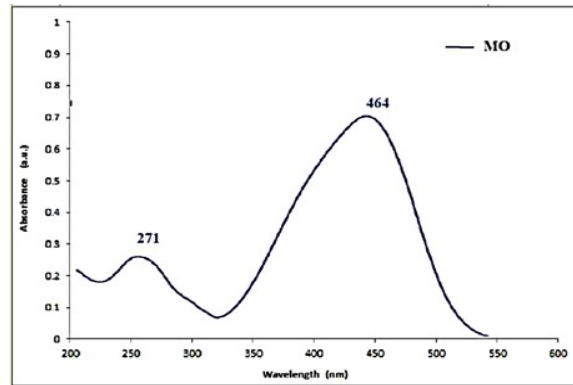


Figure 5: Absorption spectrum of MO dye

The MO is a wavelength of 464 nm. These results show that dyes are slightly affected by the ultraviolet radiation in the absence of a catalyst. Methyl Orange solution (MO) was evaluated with the presence or absence of a thin film. An aluminum plate was used as a cathode electrode, and the evaluation was made to study the efficiency of the thin films of CdS in photocatalytic activities. A surface with an area of 2 cm² was used as a catalyst of CdS thin film. As the nanoparticles were installed on it and adhered well, it was placed into a 100 ml beaker of MO solution. The photoreactor equipment and mercury lamp (100 W) without cover glass as a source for UV irradiation were used to determine the degradation efficiency degree of the time period from 0 to 240 min. By measuring absorption at 464 nm, the concentration of MO was monitored in the aqueous solution. The PDE was studied according to Equation 1.

Photocatalytic degradation efficiency

$$PDE(\%) = \frac{C_0 - C}{C_0} \times 100\% \quad (1)$$

Expressing MO concentration by C at the reaction time t (min), the initial concentration (mg/L) of MO is C₀. It found the photocatalytic degradation rates of different dyes follow the Langmuir–Hinshelwood (L–H) kinetics model below Equation 2 [24].

$$r = \frac{dc}{dt} = \frac{kKC}{1 + KC} \quad (2)$$

where the reaction rate constant signaled k (mgL⁻¹.min⁻¹); Adsorption coefficient the for the reactant is K (Lmg⁻¹); latterly, the reactant concentration is C (mgL⁻¹). KC was be neglected, when it is the concentration C is much small with regard to unity, and the photocatalysis can be simplified to an apparent pseudo-first-order kinetics Equation 3 and Equation 4 [25].

$$-\frac{dc}{dt} = kKC \quad (3)$$

$$\ln \frac{C_0}{c} = kKt = k_{app} \times t \quad (4)$$

where k_{app} is the apparent pseudo-first-order rate constant min⁻¹.

4.2. Degradation of MO dye in different concentrations

Figure 6 (a, b, c). show the process degradation of the MO solution, where this test uses a sample from the CdS NPs in the form of a thin film scale 2×2 cm² as a stimulating factor, It was deposited on an aluminum plate. The CdS NPs were deposited on its surface with a thickness of 200 micrometers at 2 hours of sedimentation time. By the mass difference method, the thickness of deposited materials was determined. A manual factory incubator has been used that contains a mercury lamp (Philips-Germany) without a cover. As a source of UV, at a distance of 15 cm from the sample, the MO solution was used with a 100 ml volume of the prepared MO dye at a 15 ppm concentration. The pH of the solution was 7 at room temperature. Area of catalyst was (2×2 cm²) placed in a glass beaker, the blank experiment, or dark reactions, where elimination of MO could happen by sorption due to CdS NPs and the residual –OH groups away from light, The photocatalytic decolorization efficiency (PDE) is 21% of MO dye after 240 min of adsorption from the dark reactions. In the same way, the MO dye is placed in the incubator with a concentration of 15 ppm with a size of 100 ml in the beaker, and the UV rays are used without using the catalyst. The photocatalytic decolorization efficiency (PDE) is 34%, and all other parameters of the experiment remain unchanged. Various concentrations are then used (5 ppm PDE=90%, 10 ppm PDE=83%, 15 ppm PDE=75%, 20 ppm PDE=69%, 25 ppm PDE=59%) below the UV light ray with catalyst size (2×2 cm²). As it appears in Figure 6 (a), we can show the percentage of degradation reduced with rising concentration of initial MO [26]. Linear relations among ln (C/C₀) and radiation time were view under various initial MO concentrations, signaling that the reaction obeys pseudo-first-order kinetics Figure 6 (b,c).

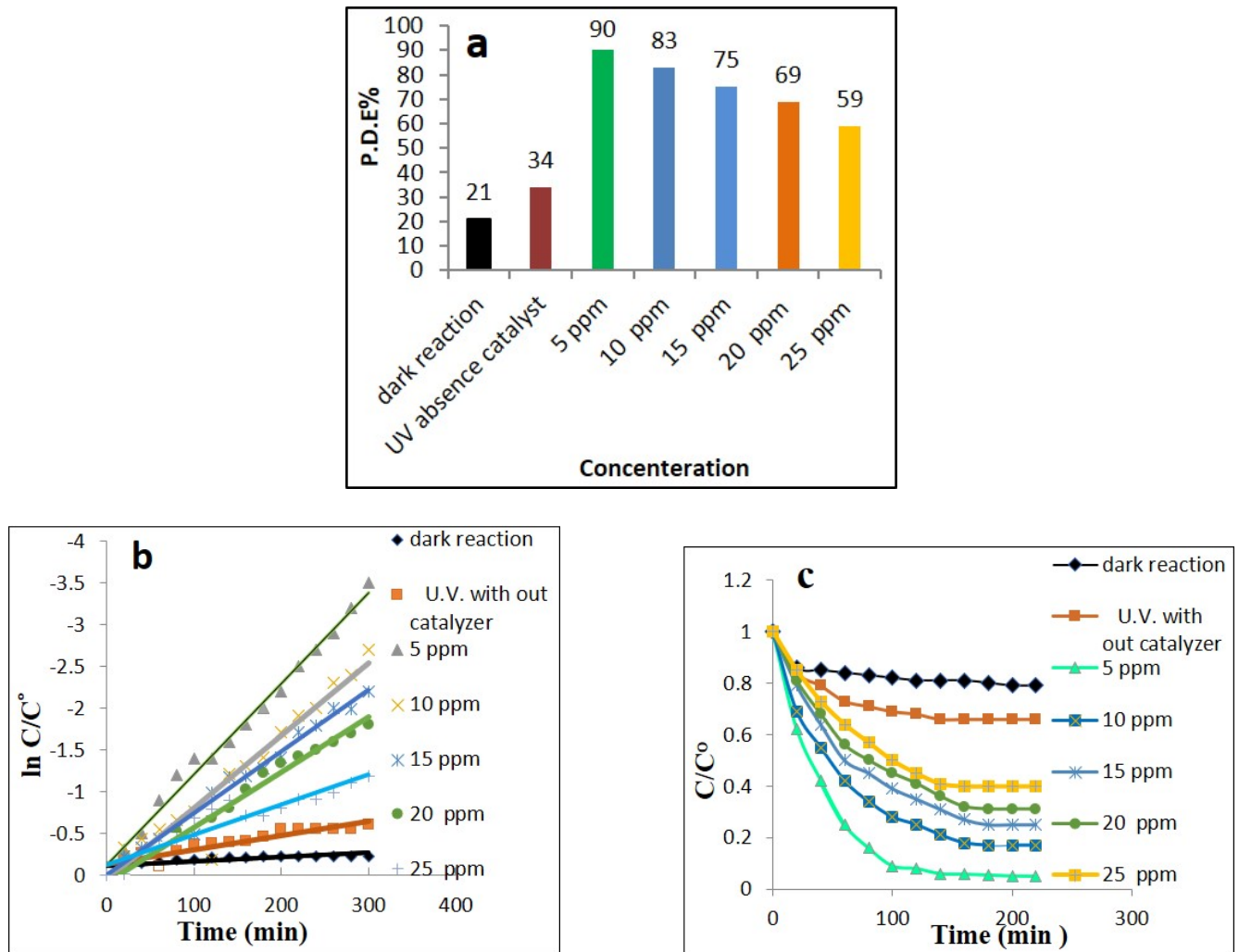


Figure 6: Effect of solution concentration on decolorization of MO (a) Photocatalytic degradation efficiency PDE %, (b) Linear relation between $\ln(C/C_0)$ and radiation time (c) Degradation efficiency on concentrations

The process of absorption and photocatalytic degradation of MO is done at the same time on the nanoparticle thin film in the existence of UV light rays. The results show that the photocatalytic degradation efficiency of low concentrations (5 ppm) is high (PDE 90%). The strength of adsorption from the CdS nanoparticle thin film promotes the photocatalytic reaction across MO decolorization, and synergistically, the adsorption and photocatalysis produce dye degradation. During the process of photocatalytic degeneration, the strong species that includes superoxide radicals ($\bullet\text{O}_2^-$), holes (h^+), and hydroxyl radicals ($\bullet\text{OH}$) with strong oxidation capacity is formed through the interaction. To discover the active species through photocatalytic operation, the effective $\bullet\text{OH}$, such as known holes and $\bullet\text{O}_2^-$ scavengers, respectively, During the photocatalytic decomposition process, it is combined with the MO solution in the court experience. In variance, the concentration of 25 ppm has a lot passive impact on the degradation of MO, supported by the fact that the superoxide radicals were the predominant active species. Thus, the main photocatalytic path can be offer. primarily, the photons with the energy higher than that of the CdS band gap are absorbed onto the CdS surface. This results in the excitation of the electrons from the valence band (VB) to the conduction band (CB), fabricating holes (h_{vb}^+) at the valence band end and electrons (e_{cb}^-) in the conduction band Equation 5. Therefore, ECB is able to interact with the $\bullet\text{O}_2^-$ molecules to events O_2^- Equation 6. eventually, the oxidized MO molecules by $\bullet\text{O}_2^-$ and degeneration products Equation 7.



4.3. Concentration effect on the rate constants (k_{app}) of the degeneration of MO dye

Linear relations between $\ln(C/C_0)$ and radiation time were observed under various initial MO concentrations, signaling that the reaction followed a pseudo-1st-order reaction Figure 7. The rate constants ($k_{\text{app}} \text{ min}^{-1}$) for the degeneration method were 11, 20, 149, 88, 69, 58, and 45×10^{-4} at dark reaction, UV absence catalyst, and different concentrations under UV lighting, with the following kept by all conditions of

experiment: 5, 10, 15, 20, and 25 ppm effect of concentrations from initial MO, respectively [27]. with rising initial MO concentration, it was observed lowering the rate constant of photodegradation. Probably that as the overall dye concentration increases, the aqueous concentration of dye elevates, leading to reduced penetration of light through the solution onto the surface of the catalyst and consequently less production of hydroxyl radicals, which are primary reactive species responsible for dye decolorization [28].

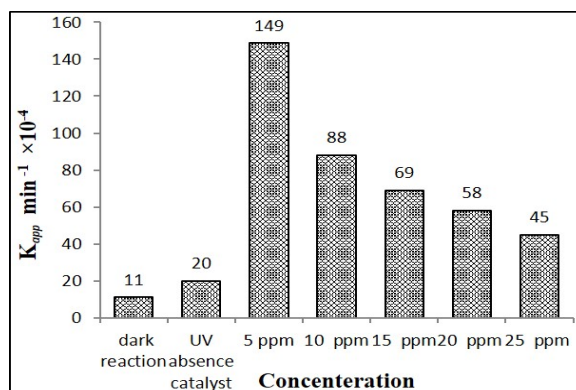


Figure 7: The rate constants (k_{app}) for the decolorization process Kinetics of Photodegradation MO dye

Through kinetic studies conducted under optimal conditions, the rates of photocatalytic degradation for MO were evaluated: from a concentration of initial dye of 5 ppm and a reaction time of 240 min, with all conditions of the experiment kept. The first-order kinetics model was used for the degradation of MO over time, with the results presented in Figure 8. The adjusted correlation coefficients of R^2 point to 0.947, and the photodegradation efficiency (PDE) of 90% indicates a vigorous model suitable for use. The calculated rate constant (k_{app}) was 0.0149 confirming that the photocatalytic degradation operation takes on first-order kinetics. The high R^2 values demonstrate that the first-order kinetic model reliably describes the fits the degradation behavior of MO.

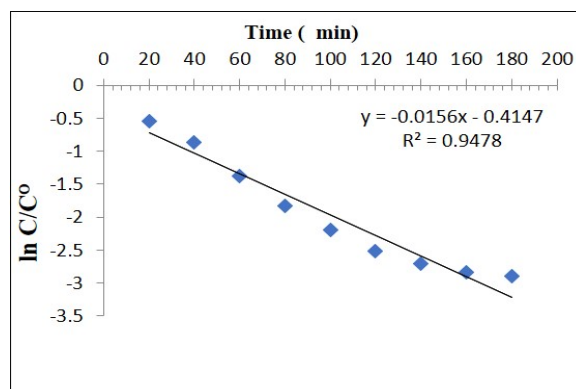


Figure 8: First-order kinetics for the degradation of MO dye at optimized parameters

4.4. The MO degradation at pH activity

The pH of the solution plays a crucial role in hydroxyl radical generation and thereby significantly influences the efficiency of dye decolorization. The photocatalytic degradation of MO solution (5 ppm) under various pH values of 3, 7, and 10 was scrupulous in this research in the existence of CdS NPs thin film Figure 9. The photodegradation efficiency at a pH of 3 and the linear relation among the $\ln(C/C_0)$ and radiation time were obviously under various initial pH levels. The rate constants (k_{app}) for the degradation method reduced from $0.43 \times 10^{-2} \text{ min}^{-1}$ at pH 3 to $0.29 \times 10^{-2} \text{ min}^{-1}$ at pH 7 and to $0.17 \times 10^{-2} \text{ min}^{-1}$ at pH 10. demonstrating that the photocatalytic removal of MO was most efficient in the acidic media. An MO molecule with a sulfuric group normally exists as an anion. The isoelectric point of CdS is near 5.5 [29, 30] the surface was positively charged in the acidic solution, which could promote the anionic MO sorption during electrostatic interactions and next degradation and increase the sorption of dye anions. The adsorbed anions of MO could be oxidized straight through hydroxyl radicals generated in the existence of a photocatalyst.

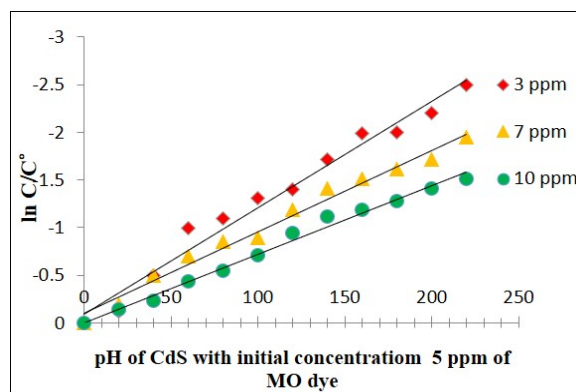


Figure 9: pH of CdS with an initial concentration of 5 ppm of MO dye

5. Conclusions

In this study, nanoparticles were prepared for the CdS that was deposited on the aluminum pole to form a thin layer of nanoparticles of the CdS ($2 \times 2 \text{ cm}^2$), and the thickness of the fine layer was $200 \mu\text{m}$. And at the same time, a few sediments were obtained at the bottom of the glass cell. Several tests have been conducted using different techniques to determine surface morphology and size of nanoparticles. The structural characterization and surface morphology were studied by XRD, UV, EDX, and SEM. The thin film can be utilized effectively for MO photodegradation efficiency under the UV light radiation. The photocatalytic operation obeys apparent pseudo-first-order kinetics. The degradation of the MO solution was highly efficient in the acidic medium.

Article Information

Conflict of benefit : The authors announce that they have no interest in this work or contradict any person or institution.

Disclaimer (Artificial Intelligence): The author(s) hereby declare that NO generative AI technologies such as Large Language Models (ChatGPT, COPILOT, etc.), and text-to-image generators have been used during writing or editing of manuscripts.

Competing Interests: Authors have declared that no competing interests exist.

References

- [1] Kavinkumar Ravikumar and Milind Shrinivas Dangate. Advancements in stretchable organic optoelectronic devices and flexible transparent conducting electrodes: Current progress and future prospects. *Heliyon*, 10(13):e33002, 2024.
- [2] Francesco Tavella and Claudio Ampelli. Electrode and cell engineering for advancing photo-electrochemical (PEC) solar fuel production. In *Proceedings of Catalyst Design Strategies for Photo-and Electrochemical Fuel Synthesis (ECAT25)*, 2024.
- [3] A. S. Lahewil, Y. Al-Douri, U. Hashim, and N. M. Ahmed. Structural, analysis and optical studies of cadmium sulfide nanostructured. *Procedia engineering*, 53:217–224, 2013.
- [4] O. K. Echendu, S. Z. Werta, F. B. Dejene, and K. O. Egbo. Structural, vibrational, optical, morphological and compositional properties of CdS films prepared by a low-cost electrochemical technique. *Journal of Alloys and Compounds*, 778 :197–203, 2019.
- [5] G. Murali, D. A. Reddy, S. Sambasivam, R. P. Vijayalakshmi, and V. Rajagopal Reddy. CdS microflowers and interpenetrated nanorods grown on Si substrate: structural, optical properties and growth mechanism. *Mater. Chem. Phys.*, 146:399–405, 2014.
- [6] D. A. Reddy, J. Choi, S. Lee, Y. Kim, S. Hong, D. P. Kumar, and T. K. Kim. Hierarchical dandelion-flower-like cobalt-phosphide modified CdS/reduced graphene oxide- MoS₂ nanocomposites as a noble-metal-free catalyst for efficient hydrogen evolution from water. *Catal. Sci. Technol.*, 6:6197–6206, 2016.
- [7] L. Cheng, Q. Xiang, Y. Liao, and H. Zhang. CdS-based photocatalysts. *Energy Environ. Sci.*, 11:1362–1391, 2018.
- [8] X. Yu, N. Ren, J. Qiu, D. Sun, L. Li, and H. Liu. Killing two birds with one stone: to eliminate the toxicity and enhance the photocatalytic property of CdS nanobelts by assembling ultrafine TiO₂ nanowires on them. *Sol. Energy Mater. Sol. Cells*, 183:41–47, 2018.
- [9] Y. Hu, Y. Liu, H. Qian, Z. Li, and J. Chen. Coating colloidal carbon spheres with CdS nanoparticles: microwave assisted synthesis and enhanced photocatalytic activity. *Langmuir* 26, pages 18570–18575, 2010.
- [10] E. Haque, J. W. Jun, and S. H. Jung. Adsorptive removal of methyl orange and methylene blue from aqueous solution with a metal-organic framework material, iron terephthalate (MOF-235). *J. Hazard. Mater.*, 185:507–511, 2011.
- [11] K. Kalpana and V. Selvaraj. Thiourea assisted hydrothermal synthesis of ZnS/CdS/Ag₂S nanocatalysts for photocatalytic degradation of Congo red under direct sunlight illumination. *RSC Adv.*, 6:4227–4236, 2016.

- [12] T. Chen, Y. Zheng, J. Lin, and G. Chen. Study on the photocatalytic degradation of methyl orange in water using Ag/ZnO as catalyst by liquid chromatography electrospray ionization ion-trap mass spectrometry. *J. Am. Soc. Mass Spectrom.*, 19:997–1003, 2008.
- [13] S. Chen, J. Zhang, C. Zhang, Q. Yue, Y. Li, and C. Li. Equilibrium and kinetic studies of methyl orange and methyl violet adsorption on activated carbon derived from *Phragmites australis*. *Desalination*, 252:149, 2010.
- [14] K. Kalpana and V. Selvaraj. Thiourea assisted hydrothermal synthesis of ZnS/CdS/Ag₂S nanocatalysts for photocatalytic degradation of Congo red under direct sunlight illumination. *RSC Adv.*, 6:4227–4236, 2016.
- [15] Z. Khan, T. R. Chetia, A. K. Vardhaman, D. Barpuzary, C. V. Sastri, and M. Qureshi. Visible light assisted photocatalytic hydrogen generation and organic dye degradation by CdS–metal oxide hybrids in presence of graphene oxide. *RSC Adv.*, 2:12122–12128, 2012.
- [16] A. S. Mandawade et al. *Synthesis And Structural Characterization Of Cadmium Sulphide (CdS) Thin Film by Electrochemical Deposition Of Two Electrode System*. 2018.
- [17] K. He, N. Chen, C. Wang, L. Wei, and J. Chen. Method for determining crystal grain size by x-ray diffraction, journal = Crystal Research and Technology. 53:2, 2018. 1700157.
- [18] N. K. H. S. Hakeem and Abbas. Preparing and studying structural and optical properties of Pb_{1-x}Cd_xS nanoparticles of solar cells applications. *Baghdad Science Journal*, 18:640–648, 2021.
- [19] R. Ranjana, C. M. S. Negib, and K. P. Tiwary. Synthesis of Mn²⁺ modified CdS nanoparticles and its application as catalyst in photodegradation of methyl red dye. *Chalcogenide Letters*, 20(4):251–259, 2023.
- [20] Nada K. Abbas and Zainab Yaaqoub. Effect of using different preparation methods on the properties of cds nanoparticles. *Iraqi Journal of Industrial Research*, 9(3):78–88, 2022.
- [21] S. Xie, P. Huang, J. J. Kruzic, X. Zeng, and H. Qian. A highly efficient degradation mechanism of methyl orange using Fe-based metallic glass powders. *Scientific reports*, 6:1, 2016. 21947.
- [22] M. R. Al-Mamun, K. T. Hossain, S. Mondal, M. A. Khatun, M. S. Islam, and M. Z. H. Khan. Synthesis, characterization, and photocatalytic performance of methyl orange in aqueous TiO₂ suspension under UV and solar light irradiation, journal = South African Journal of Chemical Engineering. 40(1):113–125, 2022.
- [23] Veera Prabakaran Elanjitsenni and Senthil Vadivu Kulandhaivelu. Unveiling the novel anti-corrosion and anti-bacterial biofilm forming characteristics of eco-safe MWCNT-AZ91E alloy for food-processing surfaces. *Bulletin of the Chemical Society of Ethiopia*, 2024:38, 1897-1914. 6.
- [24] Moussa Abbas and Mohamed Trari. Contribution of photocatalysis for the elimination of Methyl Orange (MO) in aqueous medium using TiO₂ catalyst, optimization of the parameters and kinetics modeling. *Desalination and Water Treatment*, 214:413–419, 2021.
- [25] Benali O. Benyahia M. Benmoussa Y. Zenasni Meroufel, B. M. A. Adsorptive removal of anionic dye from aqueous solutions by Algerian kaolin: Characteristics, isotherm, kinetic and thermodynamic studies. *J. Mater. Environ. Sci.*, 4(3):482–491, 2013.
- [26] R. Jiang, H. Zhu, G. Zeng, L. Xiao, and Y. Guan. Synergy of adsorption and visible light photocatalysis to decolor methyl orange by activated carbon/nanosized CdS/chitosan composite. *J. Cent. South. Univ. T.*, 17:1223–1229, 2010.
- [27] H. Zhou, H. Wang, C. Yue, L. He, H. Li, and Ma T. Zhang, H. *Photocatalytic degradation by TiO₂-conjugated/coordination polymer heterojunction: Preparation, mechanisms, and prospects*. Applied Catalysis B: Environment and Energy, 344: 123605, 2024.
- [28] M. Abdu, S. Tibebe, S. Babae, A. Worku, T. A. Msagati, and J. F. Nure. Optimization of photocatalytic degradation of Eriochrome Black T from aqueous solution using TiO₂-biochar composite. *Results in Engineering*, 25:104036, 2025.
- [29] M. A. Farwa U. Nasr S. Yahia I. S. Fatima S. Ashraf H.S andhu Z. A., Raza. Response surface methodology: a powerful tool for optimizing the synthesis of metal sulfide nanoparticles for dye degradation. *Materials Advances*, 4(21):5094–5125, 2023.
- [30] Haewon Byeon et al. Evaluation of physiochemical and electrochemical behaviour of reduced graphene functionalized copper nanostructure as an effective corrosion inhibitor. *Bulletin of the Chemical Society of Ethiopia*, 38(1):269–280, 2024.